Chemical and structural changes of quartz surfaces due to structuring by laser-induced backside wet etching

G. Kopitkovas,†[a] V. Deckert,[b] T. Lippert,*[a] F. Raimondi,‡[a] C. W. Schneider[a] and A. Wokaun[a]

Received 4th January 2008, Accepted 18th March 2008
First published as an Advance Article on the web 17th April 2008
DOI: 10.1039/b800090e

Various physical and chemical processes which are involved in laser-induced backside wet etching are investigated. The surface of quartz etched by the laser-induced backside wet etching using a XeCl excimer laser at various fluences is analyzed by Raman microscopy, X-ray photoelectron spectroscopy and fiber-tip attenuated total-reflection Fourier-transform infrared spectroscopy. The investigations reveal the formation of a high amount of amorphous carbon deposits at low laser fluences, which strongly adhere to the quartz surface. Combining X-ray photoelectron spectroscopy and Fourier-transform infrared spectroscopy reveals that the quartz is also chemically and structurally modified due to a loss of oxygen and by a change of the quartz polymorph at intermediate and high laser fluences. These modification and their differences for different fluences are explained by the etching mechanisms itself, *i.e.* different magnitudes of temperature and pressure jumps. The results show clearly which conditions for etching must be applied to machine high-quality structures, *e.g.* micro-optical elements in quartz.

Introduction

The recent development of small, high-power laser diodes and the miniaturization of optoelectronic devices for industrial application require micro-optical components fabricated using UV-transparent glasses such as quartz. Micro-optical components utilizing UV-transparent materials are widely used as optical connectors in telecommunication, imaging, wave-front measurements and beam homogenizers.[1–3] The most established techniques for micro-optics fabrication, *i.e.* smaller than one millimeter, in UV-transparent material is a combination of lithography, resist reflow, and reactive ion etching.[1,3–5] However, this technique of fabrication for optics is a complex, multiple-step process. Thus alternative techniques have been suggested to produce microstructured dielectric materials in order to utilize a simplified fabrication process.

Quartz can be directly machined with ultra-fast lasers,[6–9] vacuum-ultraviolet lasers (VUV)[10–13] or by a combination of VUV lasers with UV lasers.[13] Both approaches, however, are difficult to utilize for the fabrication of diffractive and refractive optical elements because of the femtosecond laser's small beam size, a relatively small fluence range where linear etching behavior can be obtained, and the need to use additional gas for the VUV laser-beam path.

Another approach for high-quality etching of UV-transparent material and the fabrication of micro-optical elements is an indirect laser-assisted etching. The etching of sapphire by copper-vapor laser and aqueous CrO_3 solution was reported by Dolgaev *et al.*[14,15] The etching mechanism seems to be based on the generation of a high temperature jump which results in a etched sapphire surface. A similar approach for the structuring of UV-transparent materials was developed by Wang *et al.*[16–18] This method is known as laser-induced backside wet etching (LIBWE). Conventional excimer lasers, *i.e.* XeCl (308 nm), KrF (248 nm), ArF (193 nm), as well as a quadrupled Nd:YAG (266 nm), and diode-pumped solid-state lasers are used for the LIBWE process as irradiation sources, while various organic solutions, such as: pyrene in acetone, tetrahydrofuran, toluene and cyclohexane; aqueous pyranine or naphatalene; naphthalene in methyl methacrylate; and pure toluene can be applied as etching media.[16–50]

Arrays of two-dimensional structures, micro-fluidic channels or submicron gratings were successfully fabricated by the LIBWE process in quartz.[21,25,29,46] Vass *et al.*[47,49] have succeeded in fabricating gratings with a line width as small as 104 nm by using a special interference technique utilizing prisms to achieve the necessary large angles for interference. The combination of LIBWE with diffractive gray-tone phase-mask projection opens a new way to fabricate well-defined, three-dimensional structures that can be used as beam homogenizers[36,37,44] or diffractive and refractive microlens arrays in quartz, BaF_2, and CaF_2.

One proposed mechanism for the LIBWE process is based on the strong absorption of intense laser light by an organic liquid in contact with the UV-transparent material. Rapid relaxation processes of excited dye molecules generate a fast increase of the temperature at the substrate–liquid interface which results in softening, melting or even boiling of UV-transparent materials. Such a fast temperature rise generates a shock wave in addition. The boiling of the solvent and

[a] General Energy Research Department, Paul Scherrer Institut, 5232 Villigen PSI, Switzerland. E-mail: Thomas.lippert@psi.ch
[b] ISAS—Institute for Analytical Sciences, Bunsen-Kirchhoff-Str. 11, 44139 Dortmund, Germany
† Present address: ABB, Lenzburg, Switzerland.
‡ Present address: European Patent Office, Munich, Germany.

the creation of a shock wave, or equivalently a bubble collapse, removes the softened material from the surface.[16,39,40,42,43,48,51,52] First studies on the surface modification of features etched in quartz by LIBWE suggest that no debris or modifications of quartz[18] are present. Recent studies suggest, however, that there is a formation of carbon films on the areas etched by the LIBWE process.[30,38,40,42] Furthermore, for certain fluence ranges, the etching of UV-transparent materials has been found to start after a number of repetitive laser pulses, known as an incubation effect.[38,42] A fast temperature increase and decrease can also change the material properties. Our studies of quartz surfaces using Raman microscopy, X-ray photoelectron spectroscopy (XPS) and fiber-tip attenuated total-reflection Fourier-transform infrared spectroscopy (ATR-FTIR)[53] suggest that different etching mechanisms occur at various laser fluences as presented in this paper. In addition, the presented LIBWE study establishes a fluence range suitable for the fabrication of high-quality micro-optical components in quartz.

Experimental

An experimental setup for LIBWE structuring of 25 × 25 mm quartz samples is shown in Fig. 1. A XeCl excimer laser [308 nm, 30 ns (FWHM)] with a repetition rate of 5 Hz was used as an irradiation source and 0.4 M pyrene in acetone as an etch solution.

The XeCl excimer laser beam, with a rectangular cross-section of 15 × 20 mm, passes through the dielectric attenuator plate which is continuously reducing the incoming laser beam intensity. A 5 × 5 mm square aperture selects a homogeneous part of the laser beam which is then imaged with a lens (f_{lens} = 100 mm) onto the backside of the quartz plate. The size of the square patterns etched in the quartz is 350 × 350 μm.

The laser fluences Φ applied in this experiment were varied between 0.8 and 2.4 J cm^{-2}, while the number of laser pulses varied in the range from 30 to 1000. The surfaces of the samples etched by the LIBWE process were analyzed by confocal Raman microscopy using a cw HeNe laser as the excitation source (632 nm, 30 mW). The analyzed area is approximately 1 μm^2, while the analytical depth of Raman microscopy is ≈ 1 μm. For a detailed surface analysis of the features etched in quartz by LIBWE, XPS is used with a non-monochromatic Mg K_α source. The lateral resolution is given by the aperture of the analyzer, collecting electrons within a 125 μm diameter. A special technique named fiber-tip attenuated total-reflection FTIR spectroscopy was applied in order to probe chemical modifications further inside the material (up to 5 μm). The key element of this technique is a flexible silver-halide optical fiber coupled with a FTIR-spectrometer. The optical fiber probe has a shaft containing one fiber for transmitting and one fiber for receiving infrared radiation. These two fibers are connected with the short U-shaped silver-halide fiber which is attached to the surface of the etched quartz area. The schematic of the ATR measurement system is described in more detail elsewhere.[53] The ATR spectroscopy and Raman microscopy experiments were carried out at room temperature and ambient pressure, while ultrahigh vacuum was used for the XPS measurements.

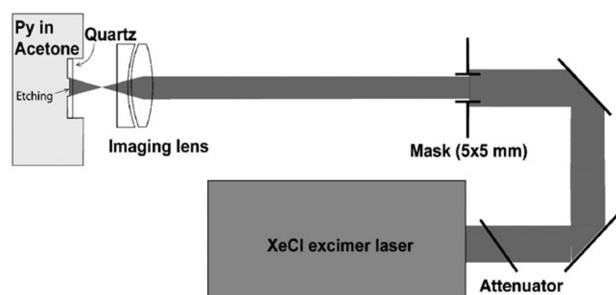

Fig. 1 Experimental setup of LIBWE.

Results and discussion

The LIBWE process is the result of a strong absorption process of incoming laser light within a very thin material–liquid layer (≤ 1 μm), here a 0.4 M pyrene-in-acetone solution on quartz.[18,20,39] Excited pyrene molecules generate a high temperature jump, which can exceed the melting temperature of the material. Within the first microsecond after the laser pulse, the temperature rises from room temperature to 2000 °C or more.[40] This fast temperature increase results in heating, melting or boiling of the surface material, followed by an explosive evaporation and also of a thermal expansion of the solution thereby generating a shock wave. This shock waves travels toward the material and solution surface and produces a sudden, strong pressure jump. Several hundred microseconds after the laser pulse, a second pressure jump is generated caused by the collapse of the laser-induced bubble.[17,20,34,40,42,48] The laser-induced pressure jumps due to shockwave expansion and bubble collapse are directed toward the molten material surface, thereby acting possibly as a "liquid" hammer which smoothly removes material off the surface.

Three fluence ranges for the LIBWE process are selected (see Fig. 3) based on etch rate, etch roughness and number of incubation pulses.[37,48] The low fluence range starts from 0.8 to 1.2 J cm^{-2}, the intermediate fluence range is from 1.2 to 2 J cm^{-2} and the high fluence range starts at fluences > 2 J cm^{-2}.

A careful balance of power with the proper solution is necessary in order to achieve the desired results. For example, using a 0.4 M pyrene-in-acetone solution with laser fluences ranging between 1.2 to 2 J cm^{-2}, the roughness of the etched features depends on the number of pulses varying from 3 to 90 nm for 10 to 90 pulses respectively.[18,20,37] Here, the roughness is defined as the root-mean-square of the deviation from the average depth as measured with a stylus instrument (DEKTAK) at the bottom of the etched patterns. This fluence range is called the intermediate fluence range and has been applied to the fabrication of three-dimensional micro-optical elements.[44,45] Laser fluences less than 1.2 J cm^{-2} induce temperatures below the quartz melting temperature but above the thermal decomposition of the solution. A product of thermal decomposition of the solution is amorphous carbon,[30,38,48] which strongly adheres to the hot quartz surface. The carbon film strongly absorbs the laser light of several successive pulses, resulting in an increase of the laser-induced temperature to temperatures above the melting temperature for

 This journal is © the Owner Societies 2008

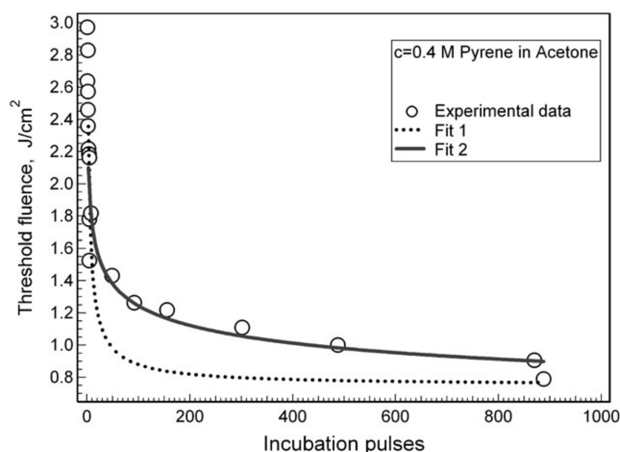

Fig. 2 Threshold fluence dependence on the incubation pulses by using 0.4 M pyrene-in-acetone solution and XeCl excimer laser (open circle). The experimental data are fitted by the model of Böhme and Zimmer[54] (dashed line) and by the model of Krüger *et al.*[55,56] (solid line).

quartz.[54] This process requires a certain number of incubation pulses to start the etching process and it leads to an increase in etch-induced roughness.[20,24,30,38] The roughness of the etched features at this fluence range is 100–300 nm for 150–1000 laser pulses respectively. A plot of the laser fluences *versus* number of incubation pulses is shown in Fig. 2 (open circles) for a 0.4 M solution of pyrene in acetone and an irradiation wavelength of 308 nm.

The formation of carbon deposits and of the incubation effect obtained in the LIBWE process was the focus of studies by Böhme and Zimmer.[54] The authors developed a model which describes the incubation effect obtained in the LIBWE process by using a KrF excimer laser (248 nm) as irradiation source and a toluene solution as etchant. The threshold fluence for a finite number of incubation pulses, $\Phi_{th}(N)$, depends on the threshold fluence obtained for a infinite number of laser pulses, $\Phi_{th}(\infty)$, where no etching occurs.[54] Within this model, the number of incubation pulse is described by

$$\Phi_{th}(N) = \frac{\Phi_{th}(\infty)}{2} + \sqrt{\left(\frac{\Phi_{th}(\infty)}{2}\right)^2 + \frac{\Phi_{th}(\infty)}{\mu N}} \qquad (1)$$

with μ the rate of photodecomposition and formation of a carbon layer, while N is the number of laser pulses. Fitting eqn (1) to our data (Fig. 2, dotted line), we obtain a threshold fluence $\Phi_{th}(\infty) = 0.75$ J cm^{-2}, even if more than 2000 pulses are applied with $\mu = 0.07$ cm^2 J^{-1}. The model seems to fit our data well for a small number of incubation pulses, whereas for larger pulse numbers there are significant deviations.

A better agreement between experiment and model description can be obtained if we consider the incubation effect for polymers with the emphasis on the carbon formation due to incubation.[55,56] The threshold fluence dependence on the number of incubation pulses is described within this model by

$$\Phi_{th}(N) - \Phi_{th}(\infty) = [\Phi_{th}(1) - \Phi_{th}(\infty)]N^{\alpha-1} \qquad (2)$$

with $\Phi_{th}(1)$ the lowest fluence at which etching occurs at the first laser pulse and $\alpha \leq 1$ represents the degree of incubation with $\alpha = 1$ corresponding to no incubation. The fit obtained agrees well with our data (Fig. 2, solid line) with $\Phi_{th}(\infty) = 0.75$ J cm^{-2}, $\Phi_{th}(1) = 3.22$ J cm^{-2} and $\alpha = 0.85$. The threshold fluence for etching obtained from the fitting is identical to the experimentally observed fluence value $\Phi_{th,exp}(1) = 3.22$ J cm^{-2} at which the etching starts with the first laser pulse. Considering the largely different boundary conditions for our experiments with respect to the model, this seems to suggest that the range of applicability (starting material, applied laser source) of the model developed by Krüger *et al.* is bigger than previously assumed.[55,56]

The LIBWE process for quartz at high fluences is not only strongly influenced by an increase of the temperature, pressure jumps and the creation of carbon deposits. The formation of a plasma is also important,[37] influencing the rapid melting/boiling and solidifying of the quartz surface at fluences higher than 2 J cm^{-2}. Therefore, the areas of quartz structured by various laser fluences reveal a different appearance as shown in Fig. 3.

A granular surface structure is found by investigating the areas etched in quartz at the low laser fluences (Fig. 3A). Optically smooth, etched surfaces are obtained for the intermediate laser fluence range (Fig. 3B), while surfaces etched at the highest laser fluences are tessellated with features typically obtained for fast melting, boiling and re-solidification processes (Fig. 3C).

The areas structured by the LIBWE process at various laser fluences were investigated by confocal Raman microscopy (Fig. 4). The areas marked in Fig. 3 from 1 to 4 correspond to the corner and center of the etched structures obtained at 0.8 J cm^{-2} (1 and 2 respectively) and at 1.5 J cm^{-2} (3 and 4 respectively), while the center of the feature structured with 3 J cm^{-2} is labeled as 5.

The Raman spectra of unstructured and structured areas indicated in Fig. 3 are shown in Fig. 4. In addition, a spectrum of an unstructured area is taken as a reference. The Raman spectrum of the area structured with 3 J cm^{-2} shows a slight

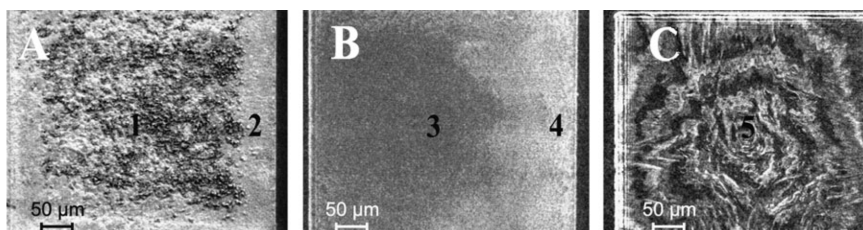

Fig. 3 Scanning electron microscope images of surface features in quartz etched by LIBWE using 0.4 M pyrene-in-acetone solution at different XeCl excimer laser fluences and different laser pulse numbers: 0.8 J cm^{-2}, 3000 pulses (A), 1.5 J cm^{-2}, 60 pulses (B) and 3 J cm^{-2}, 10 pulses (C).

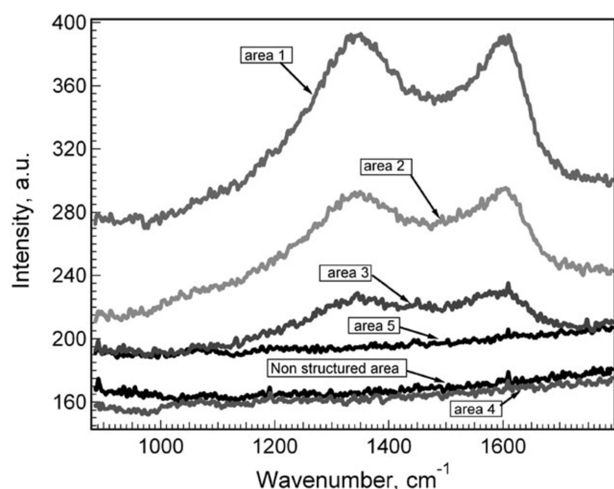

Fig. 4 Raman spectra of the etched areas in quartz by LIBWE using 0.4 M pyrene-in-acetone solution.

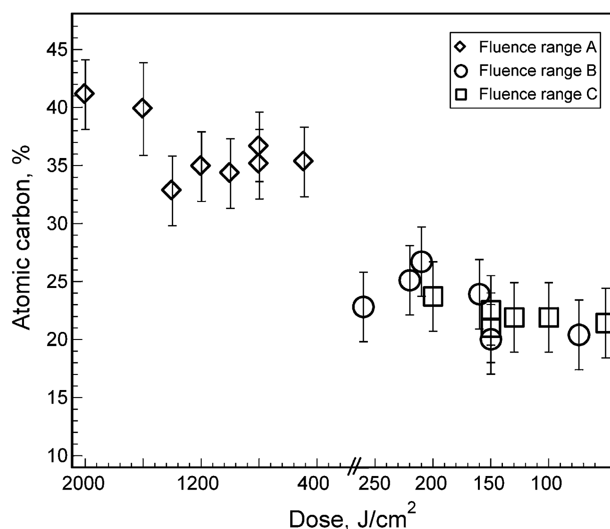

Fig. 5 Concentration of carbon on the surface of the etched areas in quartz by LIBWE evaluated from the XPS measurements.

increase of the baseline compared to the spectrum obtained for the unstructured area. This increase is likely to be caused by an enhancement of scattered laser light due to the observed increase in surface roughness. The Raman spectrum measured in the center of the etched feature at a fluence of 1.5 J cm^{-2} (area 4) is similar to the spectrum of the non-ablated surface while the spectrum of the structure in the corner etched at the same laser fluence (area 3) reveals two Raman bands at 1340 cm^{-1} and 1600 cm^{-1}. The intensity of these bands increases for areas etched at a low laser fluence 0.8 J cm^{-2} (area 1 and area 2). The Raman peaks at 1340 cm^{-1} and 1600 cm^{-1} are associated with amorphous carbon with a high bond-angle disorder, labeled carbon D and G bands.[57] This confirms the existence of amorphous carbon deposits strongly adhering to the quartz surface. The Raman analysis of the quartz surfaces structured by LIBWE with different laser fluences further suggests that layers of amorphous carbon are primarily formed at the lower and intermediate fluence range, whereas little or no amorphous carbon is found for areas structured at high laser fluences. The decomposition of the solution, however, occurs at all laser fluences because the laser-induced temperature at the quartz–liquid interface is always well above the thermal decomposition temperature of the solution. The likely reason why only little or no amorphous carbon is detected on the areas etched by using high laser fluences is an efficient plasma-mediated etching process with etch rates of up to 20 nm per pulse and a very low number of incubation pulses. Raman spectra, however, do not provide reliable information on the absolute amount of amorphous carbon and may also not be sensitive enough to very thin layers, as the analytical depths is ≈ 1 μm. The concentration of atomic carbon at the surface of the etched features was therefore measured by XPS (Fig. 5).

The laser doses, $N\Phi$, used for intermediate and high laser fluences differ from those applied for the low fluence range due to the incubation effect where etching occurs only after hundreds of repetitive laser pulses[37] For comparison, a limited number of laser pulses, typically 200, are applied at intermediate and high laser fluences due to the risk of breaking the quartz. The concentration of the atomic carbon for all areas etched is higher compared to a non-structured quartz plate, which we estimated to be less than 9% and results from air contamination. An enhancement of the carbon concentration in areas etched with the intermediate and high laser fluences suggests that the thermal decomposition of the solution occurs for all applied laser fluences; however, the concentration of carbon is highest on surfaces etched with the low laser fluences.

There are several explanations why carbon films are obtained at the surface of structures etched with the fluences from the intermediate and high fluence range (labeled B and C in Fig. 5). For these fluence ranges, quartz etching starts after several, typically three to five repetitive laser pulses. The carbon films created during these incubation pulses are very thin and strongly adhere to the very hot/molten quartz surface. They are likely to be removed together with the quartz by the strong pressure jump generated at the quartz–liquid interface. This pressure jump decays very rapidly while the temperature decay is much slower, *i.e.* a temperature of more than 500 °C will persist for up to 100 μs after the initial laser pulse.[40] Such temperatures are high enough to decompose acetone and/or pyrene which results in carbon deposits at the still-hot quartz surface. This would explain the generation of carbon films on areas etched with intermediate and high laser fluences.

Considering the fact that laser doses for the low and high laser fluences are different, it is reasonable to assume that the amount of carbon obtained on the etched surface obtained with the low laser fluence will be higher compared to that observed at the intermediate and high laser fluences. This observation agrees also with the results obtained from Raman spectroscopy measurements.

A fast temperature rise and decay and large pressure jumps at the material–liquid interface generated in the LIBWE process cause not only etching and formation of carbon deposits, but also an alteration of the structure and chemical composition of the quartz itself. Changes in quartz composition with respect to the above-mentioned etching conditions

This journal is © the Owner Societies 2008

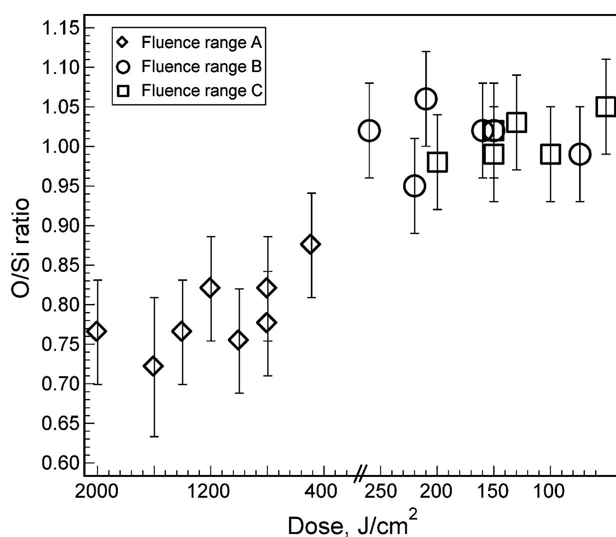

Fig. 6 Oxygen : silicon atomic ratio of quartz structured by LIBWE at various laser fluences.

are investigated by XPS. Here, we studied the atomic oxygen to silicon ratios (O : Si) and the change in binding energy of the O1s and Si2p peak as a function of the laser dose (Fig. 6 and 7). No sputter-cleaning of the surface prior to the XPS measurements has been done.

We observe that the O : Si ratio strongly decreases with increasing laser dose (Fig. 6) up to a factor of two as compared to the ratio for a non-irradiated surface (not shown here). These significant changes in the O : Si ratio suggest that for all fluences used, there is a laser-induced modification of the quartz surface. The structures etched with the low laser fluences reveal a more pronounced reduction of the oxygen content as compared to the structures etched at intermediate and high laser fluences. A high amount of carbon deposits for the low fluence range will attenuate the inelastic free path of the O1s electrons more than that of the Si2p electrons.

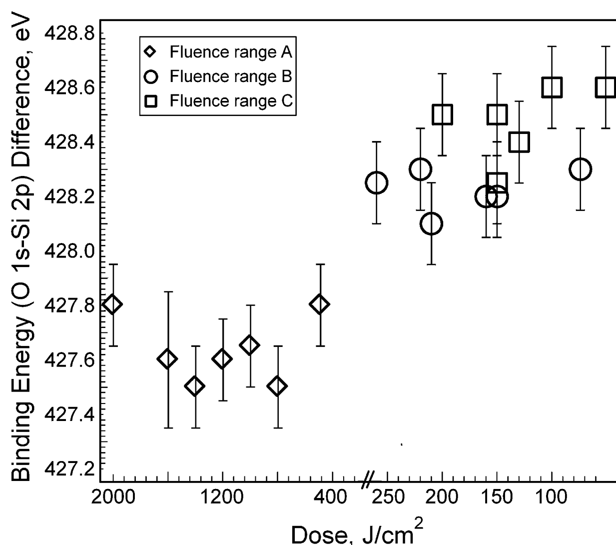

Fig. 7 The O1s–Si2p binding-energy difference of the etched areas in quartz by LIBWE.

However, the carbon deposit alone cannot be responsible for the measured low O1s : Si2p intensity ratios, because a much larger carbon concentration should be present in this case. To explain the measured intensity ratios, a partial reduction of the quartz has to take place. A strong indication of loss of oxygen in the quartz structure is associated with the measured shift of the Si2p peak to lower binding energies.[58] The observed shift of up to 0.9 eV (not shown here, the shift does not follow strictly a trend due to charging effects) would correspond to a nominal chemical composition of $\sim SiO_{1.16}$.[58] This could be interpreted that the surface layer probed (several nm) consists of a mixture best described as $(SiO)_x$ or even SiO_xC_y : H. However, it is beyond the scope of this study to quantify which $(SiO)_x$ or other modifications have actually been formed. It is also reasonable to assume that the quartz further away from the surface is likewise chemically or structurally altered due to the larger thermal gradient in the quartz during the laser-induced etch process. Therefore other origins of the shift of the binding energy, such as structural changes of the quartz to a different polymorph, should also be considered.

The information to determine possible alterations of the quartz surface and the creation of other quartz polymorphs is related to the solidification process. Several quartz phases occur while heating and solidifying the quartz: α-quartz (stable at room temperature up to 570 °C), β-quartz (570–870 °C), tridymite (870–1470 °C) and cristobalite (1470–1700 °C; melting point).[59] In the case of laser-induced wet etching, the temperature rise is very fast (up to 10^9 °C s^{-1}), therefore detecting the phase transitions of quartz during the laser-heating process is difficult. At conventional cooling rates (100 °C min^{-1}), quartz stabilizes in the α-quartz phase; however, metastable silica phases are also common.[59,60] For instance, both cristobalite and tridymite phases occur as metastable modifications at room temperature. The tridymite phase can be created during fast melting and solidifying processes which take place during the LIBWE process. The fast melting originates from the temperature jump at the quartz–liquid interface which is formed by the strong absorption of the laser light and conversion from the light to heat process. The rapid temperature jump causes the generation of the high-pressure shock waves which travel toward the solution and toward the quartz surface. The maximum pressure jump at the quartz–liquid interface is created a few hundred nanoseconds after the temperature jump.[40] The pressure and temperature rapidly decay after the laser pulse by means of solution expansion and shock waves along the quartz surface. The temperature decay from 2000 to 500 °C and pressure from 70 to 10 MPa take place within the first 3 μs after the laser pulse[40,43] and both are probably significant enough to form tridymite.

The different quartz phases have a unique bond energy and bonding angle between the silicon and the oxygen atoms.[59] The different bond energy between oxygen and silicon in the etched areas is reflected in the difference for the O1s–Si2p binding energy (BE) (Fig. 7).

The O1s–Si2p BE data were chosen in order to reduce the uncertainties deriving from the charge-correction of the binding energy scale using the C1s peak as an internal standard. Moreover, the correlation of the O1s–Si2p BE difference with

the bond geometry in various SiO_2 phases has been reported in the literature.[61] The different quartz phases have different bonding angles between the oxygen and silicon, which range from 143° (*e.g.* α-quartz) to 180° (*e.g.* tridymite).[59] The change in symmetry results in an increase of the bond angle which is enhanced from 143° (α-quartz) to 153.4° (β-quartz). The tridymite and cristobalite phases of quartz have a very high symmetry and hence much wider Si–O–Si bond angles.

The O1s–Si2p BE for the etched samples is in the range of 428.2 eV (intermediate and high laser fluences) and up to 427.6 eV (low fluence range), which is about 1 to 1.8 eV smaller than for a non-etched reference (429.6 eV). The change of the O1s–Si2p binding energy difference between the etched areas and non-structured quartz surface would correspond to an increase of the Si–O–Si angle from 144° to more than 180°.[61] One way to confirm the change of the polymorph is rnfrared spectroscopy (IR), where certain bands are sensitive to the quartz structure and therefore the quartz polymorph.

In order to study possible modifications of quartz further away from the surface, we used fiber-tip attenuated total-reflection Fourier-transform infrared spectroscopy[53] which has a sampling depth of up to 5 μm. However, the range of sensitivity is considerably smaller. Special care was taken always to apply the same pressure to the IR probes towards the sample as this can influence the intensities as well as the penetration depth. Likewise, surface roughness will influence the ATR-IR spectra taken from the etched quartz. Spectra taken for different laser fluences are shown in Fig. 8. The number of applied laser pulses was selected to have an equal irradiation dose for all applied laser fluences.

The shape around the main peak of the IR spectra at 1000 cm^{-1} for the reference area can be assigned to an asymmetric O–Si–O stretching vibration.[60] This spectrum is qualitatively similar to spectra obtained for areas irradiated with a low laser fluences (1.2 J cm^{-2}). This suggests that there is no significant structural change within the probed sample volume. The observed shift in binding energy observed by XPS for low fluence irradiation is therefore indicative of a loss of oxygen within a very thin oxygen-deficient surface layer which is not expected to influence the measured IR spectra significantly. The differences in the shape of the main IR peak at 1000 cm^{-1} between the areas structured with the fluences of 1.5 J cm^{-2} (not shown), 2.4 J cm^{-2} and the non-structured areas, however, suggest a structural modification in the quartz. This difference could be assigned to changes in quartz phases, *i.e.* from α-quartz to tridymite. Taking the measured changes of the (O1s–Si2p) binding energy difference into account, XPS and IR measurements point towards an increase of the Si–O–Si bonding angle from 144 to 170° which is close to the values for tridymite (180°). Overall, the combined IR and XPS measurements suggest that the changes observed for intermediate and high fluences are mainly due to a loss of oxygen in addition to changes of the chemical structure, *i.e.* the quartz polymorph.

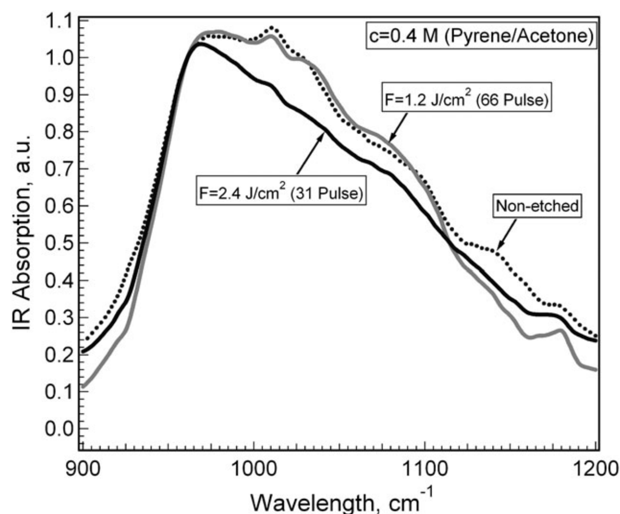

Fig. 8 Fiber-tip ATR-IR spectra of the etched areas in quartz by LIBWE at various laser fluences.

The different fluence ranges investigated have to be taken into account carefully if we consider the LIBWE process for the fabrication of micro-optical components. Quartz etching with low etch roughness is possible only when the temperature jump is above the melting point of quartz and the pressure jump is strong enough to remove molten material. Such conditions are achieved at intermediate laser fluences. Higher laser fluences induce temperatures which could exceed the boiling temperatures of quartz, thereby causing an enhancement roughness of the etched surface which is too large in order to be considered useful for the fabrication of micro-optics. The intermediate fluence range has been applied successfully to the fabrication of various diffractive and refractive optical elements;[44,48] also, small carbon deposits and chemical/structural modifications of the quartz surface are detected. This suggests that the modification and carbon deposits are not significant enough to influence the properties of the micro-optical elements, such as focal lengths or properties as a beam homogenizer.[62]

Conclusions

Laser-induced backside wet etching using pyrene solutions is a process that converts laser energy into heat due to the absorption and non-radiative relaxation of pyrene molecules. The rapid increase of the temperature at the material–liquid interface results in heating, melting or boiling of the material surface, thereby generating high-pressure shock waves. We investigated the influence of different laser fluences on the etching process and the resulting patterns have been investigated using XPS, Raman microscopy and ATR-FTIR.

For low laser fluences, the laser-induced temperature is not reaching the melting point of quartz and the generated pressure does not remove the heated material. However, the generated temperature is high enough for a thermal decomposition of the solution which generates a carbon film on the heated quartz surface. The amount of the carbon deposit grows with the number of laser pulses (typically 100–1000). Carbon, which strongly adheres to the hot quartz surface, acts as a strong light absorber. This leads to a further temperature increase thereby exceeding the melting temperature of quartz after a finite number of laser incubation pulses. The softened/molten quartz surface can now be removed by the shock-wave-

generated pressure jump. In addition, a loss of oxygen is observed in a thin quartz surface layer while no indication of a change in the chemical structure of quartz, *i.e.* the polymorph, is detected. This is attributed to the lower temperature and pressure jumps obtained for irradiation at low fluences.

The etching mechanism at intermediate and high laser fluences can be explained by the large temperature (above the melting point) and pressure jumps which remove the molten material. Etching at these fluences occurs after 1–3 repetitive laser pulses. The amounts of carbon deposited are therefore much lower compared to the low fluence irradiation. The carbon deposits are removed together with the quartz during etching and only much thinner carbon layers are formed by decomposition of the solvent/absorber at the still-hot quartz surface. The high temperature and pressure jumps and the extremely fast cooling rates very likely result in a change of the chemical structure from α-quartz to tridymite for a layer thickness in the micrometer range. An additional loss of oxygen in a thin layer seems also present.

Characterizations of micro-optic elements fabricated at the intermediate fluence have revealed no influence of the modification on their optical performance. This suggests that the LIBWE process is a very promising method for micro-optical device fabrication.

Acknowledgements

Support by the PSI is gratefully acknowledged.

References

1 S. Sinzinger and J. Jahns, *Microoptics*, Wiley-VCH GmbH & Co. KGaA, Weinheim, Germany, 2003.
2 F. M. Dickey and S. C. Holswade, *Laser Beam Shaping Theory and Techniques*, Marcel Dekker Inc., New York, 2000.
3 H. P. Herzig, *Micro-optics Elements Systems and Applications*, Taylor & Francis Ltd, London, 1997.
4 P. Nussbaum, R. Volkel, H. P. Herzig, M. Eisner and S. Haselbeck, *Pure Appl. Opt.*, 1997, **6**, 617–636.
5 H. Sankur, E. Motamedi, R. Hall, W. Gunning and M. Khoshnevisan, *Proc. SPIE–Int. Soc. Opt. Eng.*, 1995, **2383**, 179–183.
6 H. Varel, D. Ashkenasi, A. Rosenfeld, M. Wahmer and E. E. B. Campbell, *Appl. Phys. A*, 1997, **65**, 367–373.
7 J. Ihlemann, B. Wolff and P. Simon, *Appl. Phys. A*, 1992, **54**, 363–368.
8 A. Marcinkevicius, S. Juodkazis, M. Watanabe, M. Miwa, S. Matsuo, H. Misawa and J. Nishii, *Opt. Lett.*, 2001, **26**, 277–279.
9 M. Will, S. Nolte, B. Chichkov and A. Tünnermann, *Appl. Opt.*, 2002, **41**, 4360–4364.
10 J. Li, P. R. Herman, X. M. Wei, K. P. Chen, J. Ihlemann, G. Marowsky, P. Oesterlin and B. Burghardt, *Proc. SPIE–Int. Soc. Opt. Eng.*, 2002, **4637**, 228–234.
11 P. E. Dyer, A. M. Johnson, H. V. Snelling and C. D. Walton, *Appl. Surf. Sci.*, 2002, **186**, 583–587.
12 P. E. Dyer and C. D. Walton, *Appl. Phys. A*, 2004, **79**, 721–727.
13 K. Sugioka, *Rev. Laser Eng.*, 2002, **30**, 226–232.
14 S. I. Dolgaev, A. A. Lyalin, A. V. Simakin and G. A. Shafeev, *Kvantovaya Elektron.*, 1996, **23**, 67–70.
15 S. I. Dolgaev, A. A. Lyalin, A. V. Simakin and G. A. Shafeev, *Appl. Surf. Sci.*, 1996, **96–8**, 491–495.
16 J. Wang, H. Niino and A. Yabe, *Appl. Phys. A*, 1999, **69**, 271–273.
17 J. Wang, H. Niino and A. Yabe, *Appl. Surf. Sci.*, 2000, **154**, 571–576.
18 J. Wang, H. Niino and A. Yabe, *Appl. Phys. A*, 1999, **68**, 111–113.
19 J. Wang, H. Niino and A. Yabe, *Proc. SPIE–Int. Soc. Opt. Eng.*, 2000, **3933**, 64–69.
20 R. Böhme, A. Braun and K. Zimmer, *Appl. Surf. Sci.*, 2002, **186**, 276–281.
21 X. Ding, Y. Kawaguchi, H. Niino and A. Yabe, *Appl. Phys. A*, 2002, **75**, 641–645.
22 X. Ding, Y. Yasui, Y. Kawaguchi, H. Niino and A. Yabe, *Appl. Phys. A*, 2002, **75**, 437–440.
23 Y. Kawaguchi, A. Narazaki, T. Sato, H. Niino, A. Yabe, C. S. Langford and T. J. Dickinson, *Appl. Surf. Sci.*, 2002, **197–198**, 50–55.
24 Y. Yasui, H. Niino, Y. Kawaguchi and A. Yabe, *Appl. Surf. Sci.*, 2002, **186**, 552–555.
25 K. Zimmer, R. Böhme, A. Braun, B. Rauschenbach and F. Bigl, *Appl. Phys. A*, 2002, **74**, 453–456.
26 X. Ding, Y. Kawaguchi, T. Sato, A. Narazaki and H. Niino, *Chem. Commun.*, 2003, **17**, 2168–2169.
27 X. M. Ding, T. Sato, Y. Kawaguchi and H. Niino, *Jpn. J. Appl. Phys., Part 2*, 2003, **42**, L176–L178.
28 H. Niino, X. Ding, R. Kurosaki, A. Narazaki, T. Sato and Y. Kawaguchi, *CLEO/Pacific Rim 2003: The 5th Pacific Rim Conference on Lasers and Electro-Optics*, IEEE, 2003, vol. 2, pp. 742–742.
29 H. Niino, Y. Yasui, X. Ding, A. Narazaki, T. Sato, Y. Kawaguchi and A. Yabe, *Proc. SPIE–Int. Soc. Opt. Eng.*, 2003, **4977**, 269–280.
30 R. Böhme, D. Spemann and K. Zimmer, *Thin Solid Films*, 2004, **453–54**, 127–132.
31 R. Böhme and K. Zimmer, *Appl. Surf. Sci.*, 2004, **239**, 109–116.
32 X. M. Ding, Y. Kawaguchi, T. Sato, A. Narazaki, R. Kurosaki and H. Niino, *J. Photochem. Photobiol., A*, 2004, **166**, 129–133.
33 X. M. Ding, Y. Kawaguchi, T. Sato, A. Narazaki and H. Niino, *Langmuir*, 2004, **20**, 9769–9774.
34 Y. Kawaguchi, X. Ding, A. Narazaki, T. Sato and H. Niino, *Appl. Phys. A*, 2004, **79**, 883–885.
35 G. Kopitkovas, A. Chugreev, J. F. Nierengarten, Y. Rio, J. L. Rehspringer and B. Honerlage, *Opt. Mater.*, 2004, **27**, 285–291.
36 G. Kopitkovas, T. Lippert, C. David, S. Canulescu, A. Wokaun and J. Gobrecht, *J. Photochem. Photobiol., A*, 2004, **166**, 135–140.
37 G. Kopitkovas, T. Lippert, C. David, R. Sulcas, J. Hobley, A. J. Wokaun and J. Gobrecht, *Proc. SPIE–Int. Soc. Opt. Eng.*, 2004, **5662**, 515–525.
38 G. Kopitkovas, T. Lippert, C. David, A. Wokaun and J. Gobrecht, *Thin Solid Films*, 2004, **453–54**, 31–35.
39 C. Vass, B. Hopp, T. Smausz and F. Ignacz, *Thin Solid Films*, 2004, **453–54**, 121–126.
40 C. Vass, T. Smausz and B. Hopp, *J. Phys. D: Appl. Phys.*, 2004, **37**, 2449–2454.
41 K. Zimmer, R. Böhme and B. Rauschenbach, *Appl. Phys. A*, 2004, **79**, 1883–1885.
42 R. Böhme, J. Zajadacz, K. Zimmer and B. Rauschenbach, *Appl. Phys. A*, 2005, **80**, 433–438.
43 Y. Kawaguchi, X. Ding, A. Narazaki, T. Sato and H. Niino, *Appl. Phys. A*, 2005, **80**, 275–281.
44 G. Kopitkovas, T. Lippert, C. David, A. Wokaun and J. Gobrecht, *J. Laser Micro/Nanoeng.*, 2006, **1**, 23–27.
45 G. Kopitkovas, L. Urecht and T. Lippert, in *Recent Advances in Laser Processing of Materials*, ed. J. Parriere, E. Millon and E. Fogarassy, Elsevier Science, editon edn, 2006, pp. 105–135.
46 H. Niino, Y. Kawaguchi, T. Sato, A. Narazaki, T. Gumpenberger and R. Kurosaki, *J. Laser Micro/Nanoeng.*, 2006, **1**, 38–42.
47 C. Vass, K. Osvay and B. Hopp, *Opt. Express*, 2006, **14**, 8354–8359.
48 G. Kopitkovas, T. Lippert, J. Venturini, C. David and A. Wokaun, *J. Phys.: Conf. Ser.*, 2007, **59**, 526–532.
49 C. Vass, K. Osvay, B. Hopp and Z. Bor, *Appl. Phys. A*, 2007, **87**, 611.
50 K. Zimmer, R. Böhme and B. Rauschenbach, *Appl. Phys. A*, 2007, **86**, 409.
51 A. Takamizawa, S. Kajimoto, J. Hobley, K. Hatanaka, K. Ohta and H. Fukumura, *Phys. Chem. Chem. Phys.*, 2003, **5**, 888–895.
52 H. Fukumura and H. Masuhara, *Chem. Phys. Lett.*, 1994, **221**, 373–378.
53 M. H. Heise, L. Küpper, W. Pittermann and N. L. Butvina, *Fresenius' J. Anal. Chem.*, 2001, **371**, 753–757.
54 R. Böhme and K. Zimmer, *J. Phys. D*, 2007, **40**, 3060–3064.

55 S. Baudach, J. Bonse, J. Kruger and W. Kautek, *Appl. Surf. Sci.*, 2000, **154**, 555–560.
56 J. Krüger and W. Kautek, in *Polymers and Light*, ed. T. Lippert, Springer-Verlag Berlin, Berlin, editon edn, 2004, vol. 168, pp. 247–289.
57 F. Raimondi, S. Abolhassani, R. Brutsch, F. Geiger, T. Lippert, J. Wambach, J. Wei and A. Wokaun, *J. Appl. Phys.*, 2000, **88**, 3659–3666.
58 J. Finster, D. Schulze and A. Meisel, *Surf. Sci.*, 1985, **162**, 671–679.
59 P. J. Heaney, C. T. Prewitt and G. V. Gibbs, *Silica Physical Behavior, Geochemistry and Materials Applications*, Department of Geological Sciences Virginia Polytechnic Institute & State University, Blacksburg, Virginia, US, 1994.
60 J. Wong and A. C. Angell, *Glass. Structure by Spectroscopy*, Marcel Dekker Inc., New York, 1976.
61 F. J. Grunthaner, P. J. Grunthaner, R. P. Vasquez, B. F. Lewis, J. Maserjian and A. Madhukar, *Phys. Rev. Lett.*, 1979, **43**, 1683–1686.
62 G. Kopitkovas, T. Lippert, N. Murazawa, C. David, A. Wokaun, J. Gobrecht and R. Winfield, *Appl. Surf. Sci.*, 2007, **254**, 1073–1078.

 This journal is © the Owner Societies 2008